

Parametric tip model and force–distance relation for Hamaker constant determination from atomic force microscopy

C. Argento and R. H. French

DuPont Co., Central Research, E356-317A, Experimental Station Wilmington, Delaware 19880-0356

(Received 8 July 1996; accepted for publication 14 August 1996)

Hamaker constants and dispersion forces interactions of materials are of increasing interest and the advent of atomic force microscopy (AFM) force measurements represents a new opportunity for quantitative studies of these interactions. A critical problem is the determination of a force–distance relation for realistic AFM probes. Due to the inadequacies of existing power-law sphere–plane models to describe the probe–sample system, we present a new parametric tip force–distance relation (PT/FDR). A surface integration method is developed to compute the interactions between arbitrarily shaped bodies. The method is based on the Hamaker pairwise integration in a continuous fashion, reducing the six-dimensional integration to a four-dimensional scheme. With this method, the PT/FDR is obtained and a nonlinear fitting routine is used to extract the model parameters and the Hamaker constant from AFM force–distance data. From the sensitivity analysis of the fitting of synthesized AFM force–distance data, one finds that, for large tip radius (compared to separation), the force is proportional to the product of the Hamaker constant and tip radius. Unique determination of the Hamaker constant can be achieved if a small radius tip is used in the AFM scan. By fitting to literature data, the effectiveness of the PT/FDR is shown. © 1996 American Institute of Physics. [S0021-8979(96)03422-6]

I. INTRODUCTION

The van der Waals force, which arises from the interaction of oscillating dipoles, has a role in controlling many aspects of the behavior of materials. It controls or influences macroscopic phenomena such as surface tension, wetting behavior, colloidal stability, fracture, and adhesion. The van der Waals interactions can be quantified through the Hamaker constant,¹ which is a material property, and through an appropriate force–distance relation, which is dependent on the system geometry.

The determination of the Hamaker constant is an important field of research. Ackler, French, and Chiang² provide a description of the different methods available to obtain the Hamaker constant for different materials and configurations. One technique is the observation of the manifestation of these interactions on a macroscopic scale, in a phenomenological approach. For example, the surface force apparatus³ has been used to determine the interaction force between crossed cylinders with surfaces of cleaved mica. Through an analysis such as the one presented by Hamaker,⁴ the expression for the total interaction force for the specific geometry and material configuration can be calculated. Following a fit of the force–distance relation obtained experimentally, the Hamaker constant is obtained. A similar and promising new approach is the use of atomic force microscopy (AFM), due to its intrinsic capability of measuring very small forces (\sim nN) at very small separations (\sim nm).

AFM is based on the determination of the interaction force between a probe and the substrate–sample. Different kinds of interactions may be present including electrostatic (Stern *et al.*⁵), magnetostatic (Martin and Wickramasinghe⁶), and van der Waals (Weisenhorn *et al.*⁷). The van der Waals interactions are omnipresent and, for a clean, uncharged, and nonmagnetic system, it can be the only force field present. In

a procedure similar to the one described for the surface force apparatus, the Hamaker constant can be determined. So far, due to the difficulty involved in the integration to obtain the interaction force, the probe has been erroneously modeled with simple geometries, such as a sphere. The use of such models has prevented the accurate determination of the Hamaker constant for systems of interest.

The problem to be resolved can be stated as one of integrating the interaction force over the volumes of an arbitrary probe and the sample and obtaining a correct force–distance relation. Developing such an integration scheme is the main goal of this work. Initially we present the problems involved in computing the interaction force between arbitrary bodies and discuss existing results for simple geometries. We then present a surface formulation to improve the efficiency and the precision of these calculations. Following, we present a parametric model for a typical AFM probe. The interaction of this probe with a planar half-space is obtained using the surface formulation presented. We then show that the traditional power-law relation used to describe the force–distance dependence of the interaction force is inadequate since the AFM tip–substrate force–distance relation (FDR) cannot be approximated by a power law. We then demonstrate that the parametric tip–substrate force–distance relation (PT/FDR) that we develop can be used to fit (nonlinear fit) experimental data and to determine both the tip parameters and the Hamaker constant for the material configuration.

II. INTEGRATION OF THE INTERACTION FORCE

The problem of integrating the pair interaction force to obtain the total force can be approached at many different levels: the quantum-mechanical interactions between atoms; the molecular dynamic level of many atoms; or the macro-

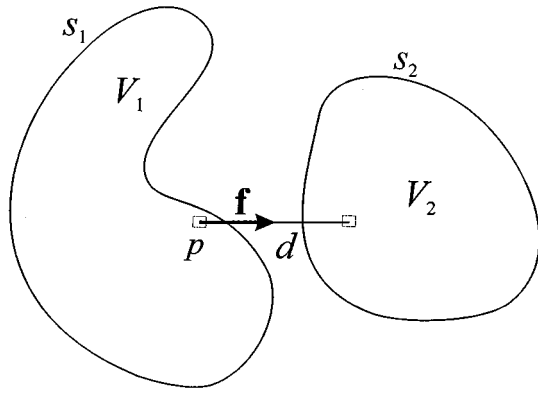


FIG. 1. Scheme for the integration of the interaction between two arbitrarily shaped bodies.

scopic (and continuous) scale. The last approach is the one used in the present work and imposes some restrictions in the dimensions of the bodies that can be considered. It is expected that it will be valid for bodies of sizes from several nanometers and larger.

Assume that the potential energy of interaction $w(d)$ is known for a pair of molecules as a function of the distance d of separation (pair potential). The interaction force between two molecules is then the gradient of the interaction potential, namely,

$$\mathbf{f} = -\nabla w. \quad (1)$$

For van der Waals interactions the potential is

$$w(d) = \frac{-C_{\text{disp}}}{d^6}, \quad (2)$$

where C_{disp} is the interaction constant as it was defined by London.⁸ In this work we adopt the usual convention that a negative force is attractive. Hamaker⁴ performed the integration of the interaction potential to compute the total interaction between macroscopic bodies. The hypotheses adopted by Hamaker were:

- additivity: the total interaction can be obtained by the pairwise summation of the individual contributions;
- continuous medium: the summation can be replaced by an integration over the volumes of the interacting bodies assuming that each ‘‘molecule’’ occupies a volume dV with a number density ρ ;
- constant material properties: the number density ρ and the interaction coefficient are constant over the volume of the bodies.

This latter assumption implies an atomically abrupt surface and that there is no retardation effects.¹⁹ Following this set of assumptions, the total interaction force between two arbitrarily shaped bodies, as shown in Fig. 1, is given by

$$\mathbf{F} = \rho_1 \rho_2 \int_{V_2} \int_{V_1} \mathbf{f}(d) dV_1 dV_2, \quad (3)$$

where ρ_1 and ρ_2 are the number densities of bodies 1 and 2. The Hamaker constant is then defined as

$$A = \pi^2 C_{\text{disp}} \rho_1 \rho_2. \quad (4)$$

The double volume integral (3) is very difficult to execute, both analytically and numerically. Hamaker⁴ obtained the interaction force for simple geometries (spheres and planar half-spaces). These geometries are of limited use, since they are not a good representation of the actual geometry involved in most physical problems.

A limited attempt to simplify the integration involved in this problem is the ‘‘Derjaguin approximation,’’ developed by Derjaguin.⁹ He proposed that two general curved surfaces could be treated as two planar half-spaces, which limits its application to surfaces with small curvatures (compared to their separation). This is clearly not the case if one considers the scale involved in AFM. This fact is discussed in more detail in the following section.

III. SURFACE FORMULATION

Our approach to deal with the problem of the complexity of the six-dimensional integration is described in detail in Argento, Jagota, and Carter¹⁰ which is summarized in this section.

From Eqs. (3) and (1) one can write

$$\mathbf{F} = -\rho_1 \rho_2 \int_{V_1} \int_{V_2} \nabla w dV_1 dV_2. \quad (5)$$

Now, let \mathbf{G} be a vector field such as

$$\nabla \cdot \mathbf{G} = -w. \quad (6)$$

Then, replacing Eq. (6) into Eq. (5) and using the divergence theorem, a double-surface integral is obtained,

$$\mathbf{F} = \rho_1 \rho_2 \int_{S_1} \int_{S_2} (\mathbf{G} \cdot \mathbf{n}_1) \mathbf{n}_2 dS_2 dS_1, \quad (7)$$

where \mathbf{n}_1 and \mathbf{n}_2 represent the normals to bodies 1 and 2. This integral produces equivalent distributed tractions over the surface of body 1 that represents a weighted average of the influence of the surface of body 2. The effective tractions replaces the actual volume field resulting in the same total interaction force. The vector field \mathbf{G} is obtained from the interaction potential of two molecules (or two infinitesimal volumes in the continuous formulation). Considering the generic potential represented by a power law

$$w(d) = -C/d^m, \quad (8)$$

where $d = (\mathbf{x} \cdot \mathbf{x})^{1/2}$ and \mathbf{x} is the vector linking a point in body 2 to a point in body 1 (interacting infinitesimal volumes in the continuous formulation) and C is an interaction constant. From Eq. (6) the solution obtained for the function \mathbf{G} is

$$\mathbf{G} = \frac{C \mathbf{x}}{(3-m)(\mathbf{x} \cdot \mathbf{x})^{m/2}}. \quad (9)$$

Using the distributive property of the divergence, expression (9) can be used to represent any potential that can be described by a series of inverse powers of degree higher than 3. The major advantage of this formulation is that the volume integration (5), which is an integration over six dimensions of a potential of degree $-(m+1)$, can be reduced to Eq. (7), a four dimensions integration of a kernel of degree $-(m$

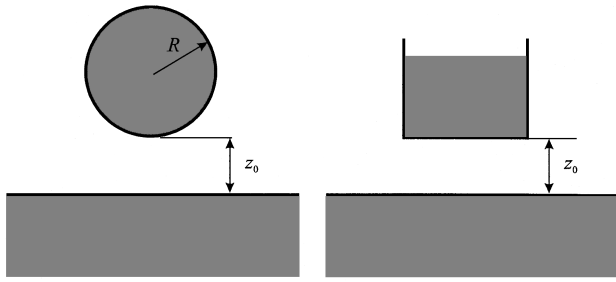


FIG. 2. Common geometrical models adopted for probe-sample system. z_0 is the separation and R is the tip radius.

– 1). This reduction in dimension and degree represents a clear advantage in analytical and numerical calculations. This surface formulation is currently being used to simulate the sintering of viscoelastic nanoparticles. It can also be used to deal with problems like adhesion, crack-tip deformations, and colloidal interactions.

IV. DEVELOPMENT OF A PARAMETRIC MODEL FOR A PROBE

Most previous work that tried to interpret the force-distance curves obtained from AFM experiments modeled the tip of the probe as a sphere or a plane surface, as shown in Fig. 2.^{2,11–14} However, the force-distance relation obtained from these models fails to describe the experimental observations. One possible reason for this fact is that the geometry proposed to describe the probe is not close to the actual one. Therefore, the force-distance relations, usually power laws, derived for these geometries are incorrect and not valid in the scale of AFM. Here we review the common sphere-plane model and present a more realistic parametric model for a typical AFM probe.

The force dependence in the case of the spherical tip and a flat sample is⁴

$$F = -\frac{2AR^3}{3z_0^2(z_0 + 2R)^2}, \quad (10)$$

where A is the Hamaker constant, z_0 is the separation between the sphere and the half-space surface, and R is the sphere radius. Assuming that the distance z_0 is small compared to the radius R , this relation is reduced to

$$F \cong -\frac{AR}{6z_0^2}. \quad (11)$$

This assumption is generally not valid if one considers the scale involved in AFM, where the tip radius can attain values of 5 nm and the separations are of the same order of magnitude. The use of Eq. (10) to describe the interaction is also erroneous, since it assumes that the sphere “floats” in space, by which we mean that its radius is large enough so that all the “nonspherical” parts of the probe are away from the region of strong interaction. The rate at which the transversal area of the probe increases with the distance from the sample has to be taken into account.

The model presented here is based on images of AFM probes obtained from scanning electron microscopy (SEM).

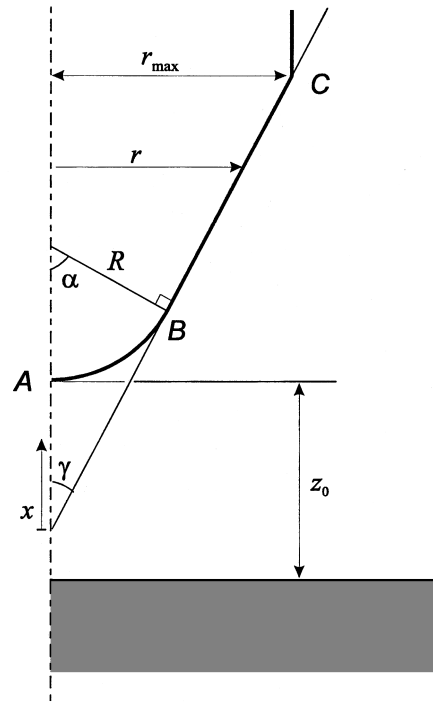


FIG. 3. Parametric tip model. R is the tip radius, r_{\max} is the radius of the cylindrical part of the probe, γ is the cone angle, $\alpha = \pi/2 - \gamma$ is the angle included in the spherical cap, z_0 is the probe-sample separation, r is the radius at any point on the surface, x is the distance from the cone apex, and A, B, and C define the spherical cap section and the conical section of the probe.

The spherical cap seems to be a good description of the tip of the probe, but the continuation of the probe should also be taken into account. Therefore, we adopt the model shown in Fig. 3. It consists of a cylinder followed by a conical section and a spherical cap. Such a model can be completely defined with three parameters: the tip radius R , the cone angle γ , and the macroscopic probe radius r_{\max} . Following we describe the integration of the interaction force for this geometry.

Let us assume that body 1 in expression (7) is the plane substrate and body 2 is the probe. We want to compute the vertical component of the interaction force, all other components being zero due to the symmetry of the problem. Therefore, $\mathbf{n}_1 = (0, 0, 1)$, and expression (7) becomes

$$\mathbf{F} = \frac{A}{\pi^2} \int_{S_2} H(z) \mathbf{n}_2 dS_2, \quad (12)$$

where

$$H(z) = \int_{S_1} \frac{-z}{(3-m)(x^2 + y^2 + z^2)^{m/2}} dx dy. \quad (13)$$

Integrating Eq. (13) over the appropriate limits for x and y , ($0 \rightarrow \infty$) yields

$$H(z) = -\frac{2\pi}{(3-m)(m-2)z^{m-3}}, \quad (14)$$

and, considering van der Waals interactions so that $m = 6$,

$$H(z) = \frac{\pi}{6z^3}. \quad (15)$$

Since we are only interested in the vertical component of the force, we shall now integrate the vertical component of Eq. (12) over the surface of the probe. Integral (12) can be broken in two different contributions, as shown in Fig. 3: the spherical cap and the remaining truncated cone. To obtain the contribution of the spherical cap first we write z as a function of z_0 and θ ,

$$z = z_0 + R - R \cos \theta. \quad (16)$$

From Eq. (15), $H(z)$ can be written as $H(\theta, z_0)$,

$$H^{\text{sc}}(\theta, z_0) = \frac{\pi}{6(z_0 + R - R \cos \theta)^3}, \quad (17)$$

where the superscript sc indicates the spherical cap. Since only the force along \mathbf{z} is being considered, the component of the normal \mathbf{n}_2 along this direction is

$$n_{2z}^{\text{sc}} = -\cos \theta. \quad (18)$$

The infinitesimal element of the surface dS_2 on the spherical cap is

$$dS_2^{\text{sc}} = 2\pi r R d\theta = 2\pi R^2 \sin \theta d\theta. \quad (19)$$

The contribution of the spherical cap to the total force is

$$F_z^{\text{sc}}(z_0) = \frac{A}{\pi^2} \int H^{\text{sc}}(\theta, z_0) n_{2z}^{\text{sc}} dS_2^{\text{sc}}. \quad (20)$$

Substituting Eqs. (17), (18), and (30) into Eq. (20) and integrating over θ from 0 to α , where α is the angle included in the spherical cap, from point A to point B in Fig. 3, produces

$$F_z^{\text{sc}}(z_0) = \frac{AR^2(1 - \cos \alpha)(R \cos \alpha - z_0 \cos \alpha - R - z_0)}{6z_0^2(R + z_0 - R \cos \alpha)^2}. \quad (21)$$

By making $\alpha = \pi$ in the above expression we obtain relation Eq. (10). Replacing $\gamma = \pi/2 - \alpha$ in expression (21), we finally obtain

$$F_z^{\text{sc}}(z_0) = \frac{AR^2(1 - \sin \gamma)(R \sin \gamma - z_0 \sin \gamma - R - z_0)}{6z_0^2(R + z_0 - R \sin \gamma)^2}. \quad (22)$$

For the contribution of the truncated cone, first we write z as a function of r and z_0 ,

$$z = z_0 + R(1 - \cos \alpha) + \tan \alpha(r - R \sin \alpha). \quad (23)$$

From Eq. (15) and after simplification, $H(z)$ can be written as $H(r, z_0)$,

$$H^{\text{cone}}(r, z_0) = \frac{\pi \cot^3 \alpha}{6[r + \cot \alpha(R + z_0 - R \sec \alpha)]^3}. \quad (24)$$

The component of the normal \mathbf{n}_2 along z for the cone is

$$n_{2z}^{\text{cone}} = -\cos \alpha. \quad (25)$$

The infinitesimal element of the surface dS_2 on the cone is

$$dS_2^{\text{cone}} = \frac{2\pi r}{\cos \alpha} dr. \quad (26)$$

The contribution of the cone section to the total force is

$$F_z^{\text{cone}}(z_0) = \frac{A}{\pi^2} \int H^{\text{cone}}(r, z_0) n_{2z}^{\text{cone}} dS_2^{\text{cone}}. \quad (27)$$

Substituting Eqs. (30), (25), and (26) into Eq. (27) and integrating over r from $R \sin \alpha$ to r_{max} , from point B to point C in Fig. 3, produces

$$F_z^{\text{cone}}(z_0) = -A \left(\frac{(r_{\text{max}} - R \sin \alpha)[2Rr_{\text{max}}(\cos \alpha - \cos 2\alpha) + 2r_{\text{max}}z_0 \cos \alpha - 2R^2 \sin \alpha + R^2 \sin 2\alpha + Rz_0 \sin 2\alpha]}{12 \sin \alpha \tan \alpha (R + z_0 - R \cos \alpha)^2 [r_{\text{max}} + \cot \alpha (R + z_0 - R \sec \alpha)]^2} \right). \quad (28)$$

It is generally reasonable to assume that r_{max} is much larger than the other dimensions of the probe, therefore, taking the limit of Eq. (28) when $r_{\text{max}} \rightarrow \infty$, we obtain

$$F_z^{\text{cone}}(z_0) = \frac{-A[z_0 \cos \alpha + R \cos \alpha - R \cos(2\alpha)]}{6 \tan \alpha \sin \alpha (z_0 + R - R \cos \alpha)^2}. \quad (29)$$

Replacing $\gamma = \pi/2 - \alpha$ we obtain

$$F_z^{\text{cone}}(z_0) = \frac{-A \tan \gamma [z_0 \sin \gamma + R \sin \gamma + R \cos(2\gamma)]}{6 \cos \gamma (z_0 + R - R \sin \gamma)^2}. \quad (30)$$

By making $R = 0$ in this expression, we obtain the expression for the force-distance relation of a sharp cone,

$$F_z^{\text{cone}}(z_0) = \frac{-A \tan^2 \gamma}{6z_0}. \quad (31)$$

V. PARAMETRIC TIP FORCE-DISTANCE RELATION (PT/FDR)

The total force on the probe, adding Eqs. (22) and (30),

$$F_z(z_0) = F_z^{\text{cone}}(z_0) + F_z^{\text{sc}}(z_0), \quad (32)$$

is

$$F_z(z_0) = \frac{AR^2(1 - \sin \gamma)(R \sin \gamma - z_0 \sin \gamma - R - z_0)}{6z_0^2(R + z_0 - R \sin \gamma)^2} + \frac{-A \tan \gamma [z_0 \sin \gamma + R \sin \gamma + R \cos(2\gamma)]}{6 \cos \gamma (z_0 + R - R \sin \gamma)^2}. \quad (33)$$

The assumptions made in the derivation of this expression are the same used by Hamaker (1937). Since there is no geometric assumption in this derivation, relation (33) gives exactly the force on the parametric probe if nonretarded Van

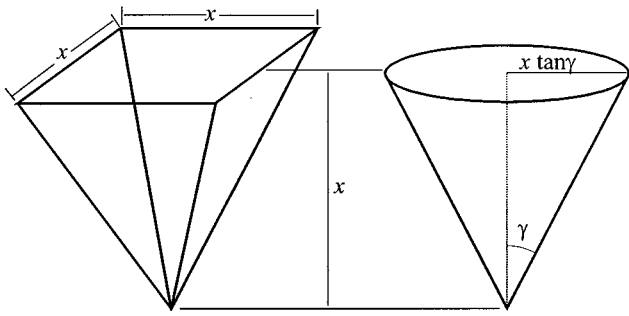


FIG. 4. Scheme for the cone with same transversal area as the pyramid probe with aspect ratio 1:1. x is the distance from the apex and γ is the cone angle.

der Waals interactions are the only interactions present. Unlike the simple power laws adopted in other works, PT/FDR does not assume that the curvature of the probe surface is small compared to the distance of separation between probe and sample. In the following section we compare PT/FDR with the traditional power-law models.

VI. ANALYSIS OF THE FORCE-DISTANCE RELATION

To determine the inadequacies of power-law models applied to AFM tips we compare them to the PT/FDR. A convenient way to do so is to analyze the force sensitivity to the distance of separation, which is the logarithmic slope of the force-distance relation. In the case of a power-law relation, the force sensitivity is identical to the exponent of the power law. The sensitivity is defined as

$$s(z_0) = \frac{\partial \ln[F_z(z_0)]}{\partial \ln(z_0)}. \quad (34)$$

The first case we are going to consider is the common pyramid probe. This probe has an aspect ratio of 1:1. The pyramidal geometry cannot be directly reproduced with the parametric model described in the previous section. To use the conical model, we should find an equivalent cone angle that will give the same transversal area for a given distance from the tip apex as for the pyramid.

In a pyramid with aspect ratio 1:1, the area of intersection of any plane parallel to the sample plane with the pyramid is simply x^2 , where x is the distance from the pyramid apex. In the cone geometry, this area is given by $\pi(x \tan \gamma)^2$, where γ is the cone angle as defined in Figs. 3 and 4. The cone angle where these two expressions are equivalent is simply given by $\gamma = \arctan \sqrt{1/\pi} = 0.5137$. This geometry is shown in Fig. 4. In Fig. 5 we plot the evolution of the force sensitivity as a function of the distance z_0 from the sample plane for different tip radii and $\gamma=0.5137$. The force sensitivity of expression (10) (sphere-plane model) is also shown. Note that, except for large radii, the force sensitivity is not uniform over the distance. This implies that the power-law representation, even for the sphere-plane model, is not valid. In some extreme cases, as when the tip radius is small compared to the separation, there is strong variation in the force sensitivity. In Fig. 6 we plot the force-sensitivity as a function of the tip radius for the parametric model and for the

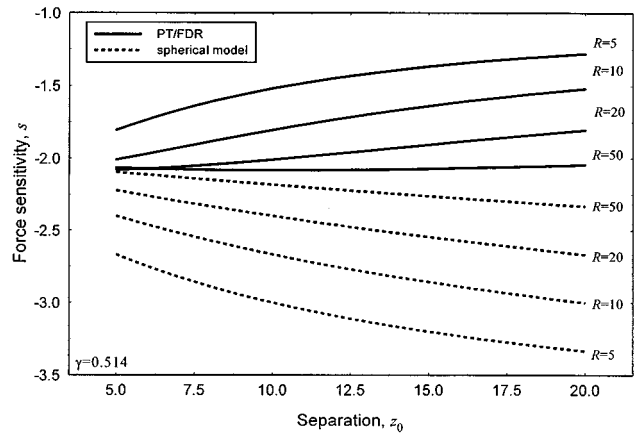


FIG. 5. Force sensitivity as a function of the separation for the PT/FDR and the spherical model for several radii R and probe angle $\gamma=0.514$. The radii and the separation are given in units of length.

sphere model for a fixed separation $z_0 = 10$ units of length. It is clear that for small tip radius the sphere model is completely wrong; however, there is some agreement in the large radius domain, which could be expected. These results should also be compared with the plane-plane model, with a force sensitivity of -3 , and with the sharp cone-plane model, expression (30), which has a force sensitivity of -1 . It is also clear that these models are unsuitable to describe the probe-sample interaction.

Another important aspect of this analysis is the sensitivity of the force-distance curve to each of the individual tip parameters. It is evident that the PT/FDR evolves toward the sphere model when the radius is increased, which can be verified in Figs. 5 and 6. The same is true in Fig. 7, where we plot the PT/FDR for several different tip radii and a fixed cone angle $\gamma=0.5137$. Note the near-constant slope for large radii and the varying slope for small radii. In the large radius domain, since the curves are parallel, the radius has a multiplicative effect on the PT/FDR, in the same way as the Hamaker constant. In Fig. 8 the PT/FDR is plotted for different cone angles and a fixed radius of 20 units of length. There is a slight change in the predicted force for small separations.

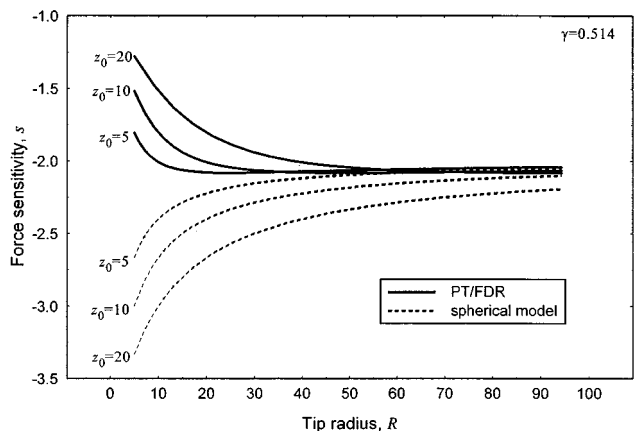


FIG. 6. Force sensitivity as a function of tip radius for the PT/FDR and the spherical model at several separations z_0 and probe angle $\gamma=0.514$. The radii and the separation are given in units of length.

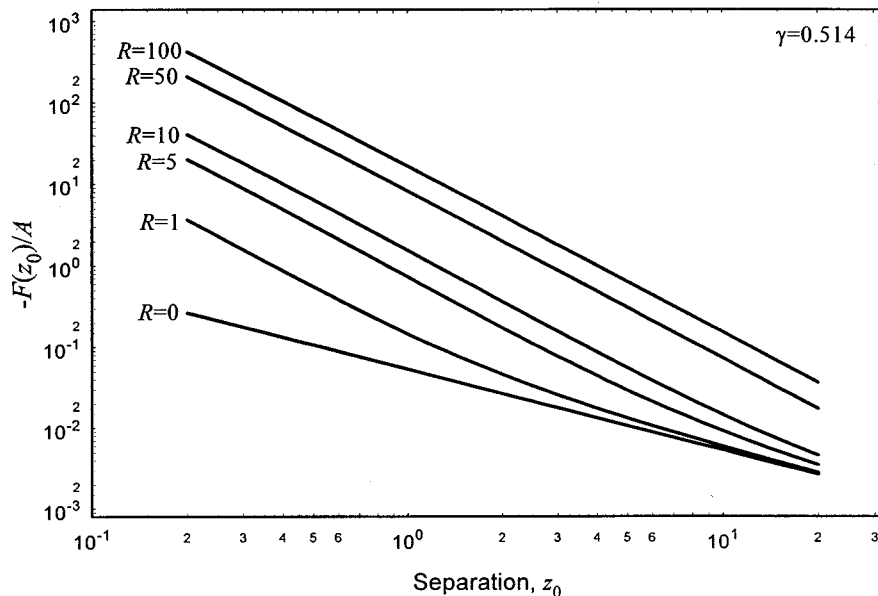


FIG. 7. Double log plot of the PT/FDR for several radii and probe angle $\gamma=0.514$. The radii and the separation are given in units of length. The vertical axis is the negative of force divided by the Hamaker constant and is given in inverse units of length.

On the other hand, at large separations, where the effect of the tip radius is diminished, the cone angle is the dominant parameter. This clearly divides the domains of importance of the parameters: close-range interaction controlled by the tip radius and long-range interaction controlled by the cone angle.

VII. NONLINEAR FITTING PROCEDURE

In this section we describe the nonlinear fitting procedure and the tests to evaluate its capability to predict the tip parameters and the Hamaker constant. Current experimental

data are inadequate to perform such evaluation since they usually contain a high noise-to-signal ratio and would lead to inconclusive results. Instead, we decide to use analytical data with artificial noise. In a first step, a number of random points is generated to represent the sampling in the distance of separation. For each of these points the force acting on the probe is calculated using the PT/FDR. The data produced this way are then perturbed by a random noise with controlled amplitude. Two cases were considered: no random noise and random noise from -10% to 10% of the maximum force on the data set. Finally, a nonlinear fitting routine is

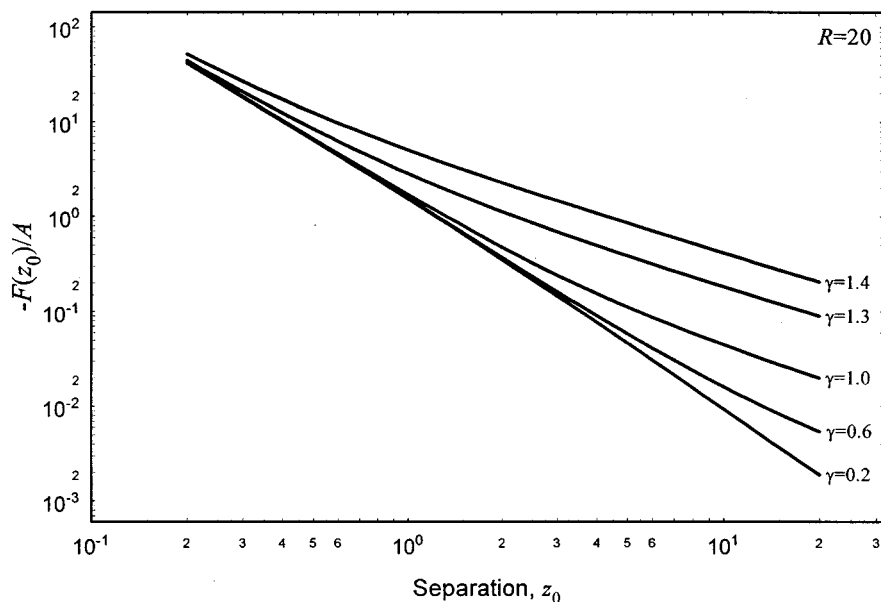


FIG. 8. Double log plot of the PT/FDR for several probe angles and tip radius $R=20$. The radii and the separation are given in units of length. The vertical axis is the negative of force divided by the Hamaker constant and is given in inverse units of length.

TABLE I. Values and errors extracted from the different fitting tests. The radius R is in units of length and the Hamaker constant A is in consistent units of energy.

	A	R	AR	γ
No noise, $R = 100$ fixed radius	$A \rightarrow 1.00$ $e = 0\%$	fixed, $R = 100$	$AR \rightarrow 100$ $e = 0\%$	$\gamma \rightarrow 0.514$ $e = 0\%$
No noise, $R = 100$ fixed angle	$A \rightarrow 0.90$ $e = -10\%$	$R \rightarrow 110.8$ $e = 10.8\%$	$AR \rightarrow 99.8$ $e = 2.5\%$	fixed, $\gamma = 0.514$
No noise, $R = 100$ all d.o.f.	$A \rightarrow 0.85$ $e = -15\%$	$R \rightarrow 118.0$ $e = 18\%$	$AR \rightarrow 99.7$ $e = -0.3\%$	$\gamma \rightarrow 0.412$ $e = -19.8\%$
10% noise $R = 100$ fixed radius	$A \rightarrow 0.99$ $e = -0.1\%$	fixed, $R = 100$	$AR \rightarrow 99.6$ $e = -0.4\%$	$\gamma \rightarrow -0.994$ $e = -293\%$
10% noise $R = 100$ fixed angle	$A \rightarrow 1.58$ $e = 58\%$	$R \rightarrow 62.82$ $e = -37.2\%$	$AR \rightarrow 99.3$ $e = -0.7\%$	fixed, $\gamma = 0.514$
10% noise, $R = 100$ all d.o.f.	$A \rightarrow 0.84$ $e = -16\%$	$R \rightarrow 117.1$ $e = 17.1\%$	$AR \rightarrow 98.0$ $e = 2.0\%$	$\gamma \rightarrow -0.324$ $e = -163\%$
No noise, $R = 5$ fixed radius	$A \rightarrow 1.00$ $e = 0\%$	fixed, $R = 5.00$	$AR \rightarrow 5.00$ $e = 0\%$	$\gamma \rightarrow 0.514$ $e = 0\%$
No noise, $R = 5$ fixed angle	$A \rightarrow 1.00$ $e = 0\%$	$R \rightarrow 5.00$ $e = 0\%$	$AR \rightarrow 5.00$ $e = 0\%$	fixed, $\gamma = 0.514$
No noise, $R = 5$ all d.o.f.	$A \rightarrow 0.98$ $e = 2\%$	$R \rightarrow 5.34$ $e = 6.7\%$	$AR \rightarrow 5.21$ $e = 4.2\%$	$\gamma \rightarrow 0.514$ $e = 0\%$
10% noise, $R = 5$ fixed radius	$A \rightarrow 0.99$ $e = -1\%$	fixed, $R = 5.00$	$AR \rightarrow 5.05$ $e = -1\%$	$\gamma \rightarrow 0.528$ $e = 2.7\%$
10% noise, $R = 5$ fixed angle	$A \rightarrow 1.03$ $e = 3\%$	$R \rightarrow 4.84$ $e = -3.3\%$	$AR \rightarrow 5.01$ $e = -0.2\%$	fixed, $\gamma = 0.514$
10% noise, $R = 5$ all d.o.f.	$A \rightarrow 1.04$ $e = 4\%$	$R \rightarrow 4.93$ $e = -1.3\%$	$AR \rightarrow 5.13$ $e = 2.6\%$	$\gamma \rightarrow 0.499$ $e = -2.7\%$

used to evaluate the parameters of the PT/FDR and these values are compared to the initial values used in the generation of the data. For the nonlinear fitting routine, we used the Levenberg–Marquardt method, as implemented in the MATHEMATICA® statistics package.¹⁵

Table I shows the results of the fitting procedure. The first set of data was constructed considering the separation from 2 to 20 units of length, a tip radius $R = 100$ units of length, the cone angle $\gamma = 0.5137$, Hamaker constant $A = 1$ unit of energy, and no random noise. Initially the tip radius was held fixed at the correct value and the Hamaker constant and the cone angle were the degrees of freedom. The fit for this case had an error of less than 0.1% for all the parameters. For the next case, where the angle was held fixed, there is a good prediction for the quantity AR . The values obtained for the Hamaker constant and the tip radius are within 10% of the correct values. When the three parameters were left as degrees of freedom, there is still a good agreement for the quantity AR , but then all the three parameters have an error of more than 10%. We notice here the effect discussed in the previous section, where the product between the Hamaker constant and tip radius is the governing parameter, when the tip radius is large. In the next set of data, a random noise going from -10% to 10% of the maximum force (calculated

at the minimum separation of 2 units of length) was added to each data point. The effect observed on the data without noise is repeated here. In all cases there is very good prediction for the quantity AR , even when all the parameters are degrees of freedom. Due to this fact, all the values for A and R that will satisfy the value for this quantity will produce good fittings. The prediction for the cone angle is very bad, even when the radius was held fixed. In the case of the large tip radius, the cone angle reflects only the information at long range and its contribution to the total force is very small, therefore being very difficult to fit. Figure 9 shows the noisy data set and the fitting for all three degrees of freedom. Notice the good fitting, even with bad predictions for A , R , and γ . This indicates that the system has redundancy, the only important parameter is the quantity AR .

The next set of data was generated under the same conditions except for the tip radius $R = 5$ units of length. The predictions for the three parameters in all cases are very good, including for the data set with noise. The contributions to the total force of the spherical and conical parts of the probe are equivalent, therefore being easier to fit. Also in this situation, the radius does not act as a multiplicative coefficient as was the case for the large radius data set. The quantity AR is not the governing parameter any more and the

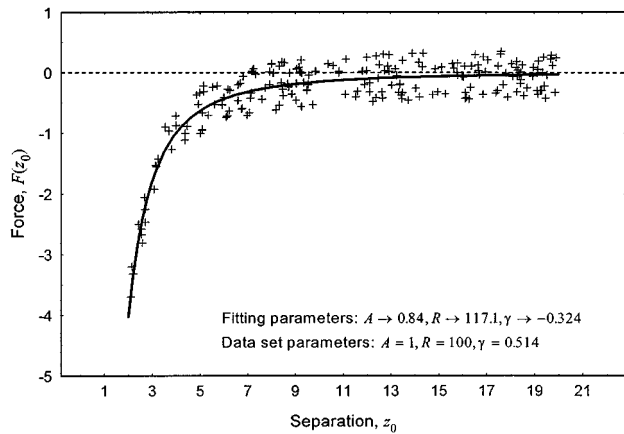


FIG. 9. Artificial data with random noise and the resulting fitting for the large radius case ($R=100$ units of length).

individual parameters have equal importance. Figure 10 shows the noisy data set and the fitting for all three degrees of freedom. This time, a good fit and good prediction for the parameters were obtained, indicating that the system is not redundant.

From this set of tests we can conclude that the fitting procedure is very efficient to extract the parameters when the tip radius is of the same, or lower, order of magnitude as the separations where the measurements are being made. In the other case, a large tip radius, the cone angle is not an important parameter and only information on the quantity AR can be accurately extracted. This is true even for the noisy data tested.

VIII. APPLICATION OF THE FITTING PROCEDURE TO EXPERIMENTAL DATA

In this section the nonlinear fitting procedure describe in the previous section is applied to two sets of experimental data. The first experiment considered was performed by Biggs and Mulvaney.¹³ They measured the force between a gold-coated AFM probe and a flat gold surface in water. The second experiment considered was performed by Ducker and

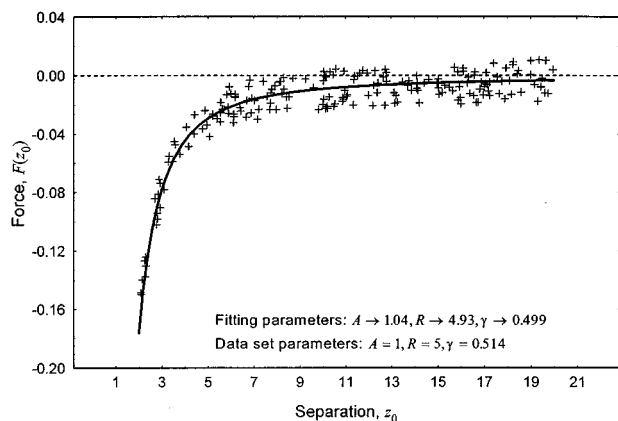


FIG. 10. Artificial data with random noise and the resulting fitting for the small radius case ($R=5$ units of length).

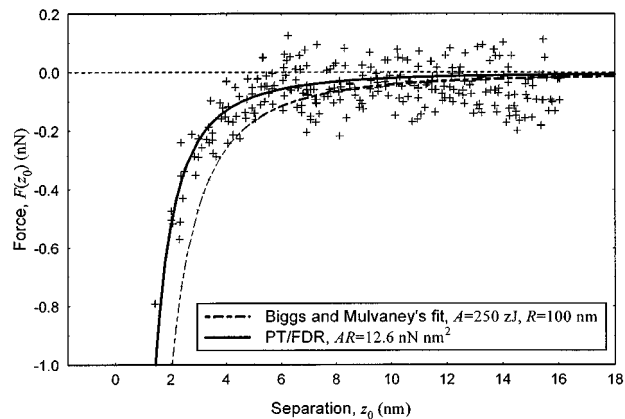


FIG. 11. Experimental data obtained by Biggs and Mulvaney (Ref. 13) and the different fittings proposed.

Clarke,^{14,16} where they obtained the force of on a silicon nitride probe interacting with a silicon nitride flat surface in water.

Biggs and Mulvaney performed two sets of experiments. In the first one, a gold-coated silica sphere was attached to the AFM cantilever. The final radius of the sphere was found to be $3.3 \pm 0.1 \mu\text{m}$. This radius places the sphere in the large radius domain and, considering the distances of separation sampled going from 9 to 100 nm, the traditional approach using the simplified power-law model can be used (except for the fact that retardation¹⁹ may be involved). The second experiment consisted of measuring the interaction force between an AFM probe coated with gold and a flat gold sample. The authors calculated an effective tip radius of 100 nm. The Hamaker constant for this configuration was obtained by Rabinovich and Churaev¹⁷ and ranges from 90 to 300 zJ, the value of 250 zJ being used by the authors as the best fit for their experimental data.

We analyzed the same experimental data under different conditions of fitting as it has been described in the previous section. The value of the force at small separations and the fact that the cone angle is a negligible parameter during the fitting indicates that the tip radius is large. Therefore, the cone angle was fixed at 0.514, which is characteristic of the cone equivalent to a pyramid with a 1:1 aspect ratio. This value had little effect on the final shape of the FDR. The values of the Hamaker constant and the tip radius fluctuated a lot under the different conditions of fitting, but we consistently extracted their product as being $12.6 \pm 0.3 \text{ nN nm}^2$. Figure 11 shows the experimental data, the fitting proposed by the authors, with a tip radius of 100 nm and a Hamaker constant of 250 zJ, and the fitting obtained with PT/FDR with $AR=12.6 \text{ nN nm}^2$. With this value and a tip radius of 100 nm, the Hamaker constant calculated would be 126 zJ. It is clear that the curve plotted with these values is in very good agreement with the experimental data. The value of 126 zJ is within the limits obtained by Rabinovich and Churaev.¹⁷ The value of 100 nm was measured by the authors using an electrostatic method proposed by Drummond and Senden,¹⁸ where the probe is modeled as a sphere. Since the actual shape of the tip is not spherical and the value of

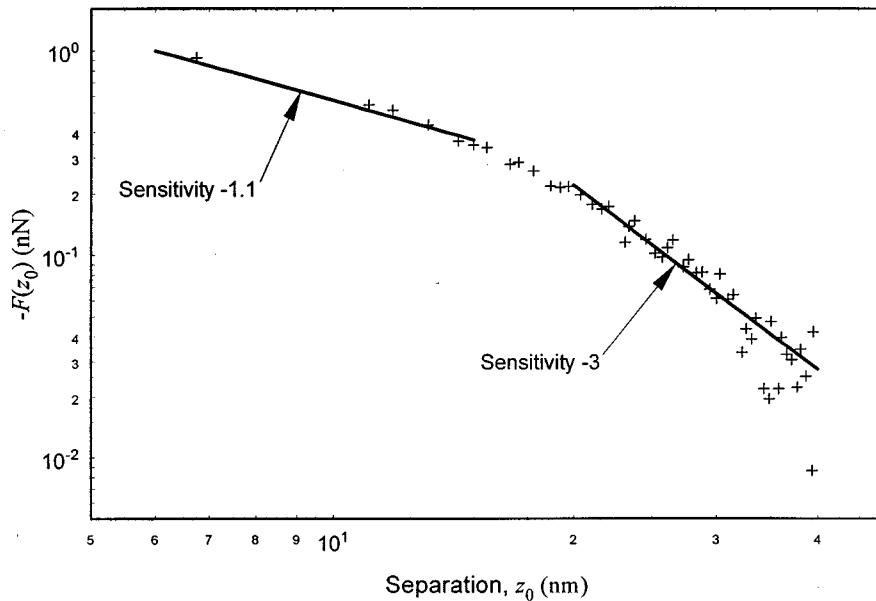


FIG. 12. Double log plot of the experimental data obtained by Ducker and Clarke (Ref. 14). The curves correspondent to force sensitivities -1.1 and -3 are also shown.

the effective tip radius given by the authors is not equivalent to the tip radius as defined in this work, some disagreement is expected.

The second set of experimental data considered here were obtained by Ducker¹⁶ as described in Ducker and Clarke.¹⁴ The data consist of force–distance points obtained with a silicon nitride probe and a flat silicon nitride sample in water, with separations ranging from 5 to 80 nm. The values for the Hamaker constant for this configuration reported in the literature range from 45 to 100 zJ.² There is no information given by the authors regarding the tip radius of the probe used; we expect it to be in the vicinity of the more common probes used today, which is 100 nm.

The first thing we notice in these data is the unusually high interaction force. With a pyramid probe and 100 nm tip radius and at the higher end of Hamaker constant for this material configuration, 100 zJ, the force calculated from PT/FDR would range from -6.37×10^{-2} nN at 5 nm to -2.20×10^{-4} nN at 80 nm. These values are far lower than the values obtained in the experiment, where the force at 5 nm is -9.26×10^{-1} nN. Another important feature of this data is its force sensitivity to distance (the log–log slope). Figure 12 shows the data in a double log plot. The sign of the force was inverted and only values representing separations from 5 to 40 nm are plotted. Notice in the figure the initial sensitivity of approximately -1.1 and its evolution to a value of -3 . This is not consistent with any of the dispersion force models described here. In the sphere model, the sensitivity ranges from -2 at close separations to -4 , which is representative of a molecule interacting with a halfspace. For the PT model the sensitivity goes from -2 at close separations to -1 at long range, which is representative of a sharp cone. There are several possible explanations for these facts. One possible cause is that the model presented here accounts only for the van der Waals forces. The model cannot repro-

duce the experiment if there is any other type of interaction present. That would be the case, for example, if other types of long-range interactions were present.

Another possible explanation for this fact is the wrong determination of the point of zero force and zero separation, what is a major problem in AFM experiments. To verify these effects, an offset was added to the distance of separation and to the total force in the PT/FDR. These two parameters were also used in the nonlinear fitting routine. In Fig. 13 the FDR thus obtained is plotted along with the data. This curve was obtained with an offset on the distance of 7.03 nm and on the force of 5.32×10^{-2} nN. As was the case with the previous example, the important parameter is the quantity AR , which was extracted as 1231 nN nm^2 . For a tip radius of 100 nm, the Hamaker constant would be $1.23 \times 10^4 \text{ zJ}$, which is far greater than expected value for this material configuration.

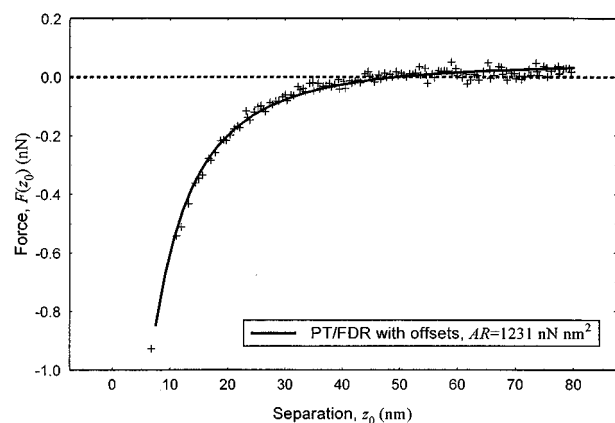


FIG. 13. Experimental data obtained by Ducker and Clarke (Ref. 14) and the fitting proposed.

IX. CONCLUSION

The main goal of this article was to introduce the force–distance relation for a realistic parametric tip, which has been successfully achieved in the form of the PT/FDR. Furthermore, the study on the numerically generated data set showed that, in the more common cases when the tip radius is large, the determination of Hamaker constant from the nonlinear fitting routine is compromised by the fact that the Hamaker constant and the tip radius are redundant parameters. In these cases, the angle of the conical part of the probe is irrelevant, especially when the data has a high noise-to-signal ratio at large separations. However, the same analysis showed that all the three parameters can be accurately extracted from the data if the tip radius is small. This is especially interesting since, in these cases, the sphere model is completely invalid. The nonlinear fitting routine is very efficient when there is no redundancy of parameters in the PT/FDR, as in the small radius regime.

The study performed on prior experimental data was not conclusive since both experiments were performed with large radius tips. In all cases we were able to produce extremely good fits to the data with the PT/FDR. The quantity AR was correctly extracted from the data set obtained by Biggs and Mulvaney¹³; however, it seems that experimental results presented by Ducker and Clarke¹⁴ cannot be accounted for by van der Waals force alone, even with the offset corrections introduced. The interaction forces in this experiment were extremely high to be described as van der Waals forces. We conclude that either there is an experimental problem or an extra attractive force.

More analysis is necessary from experiments with probes with smaller tip radius and smaller noise-to-signal

ratio. We could benefit from AFM force distance measurement in ultrahigh vacuum, where the Hamaker constant is usually large and the noise-to-signal ratio is, consequently, lower.

ACKNOWLEDGMENTS

The authors would like to acknowledge helpful discussion with D. Bonnell and W. A. Ducker. In addition, C.A. acknowledges the support of the AFOSR under Contract No. F49620-95-C-0008.

- ¹J. Israelachvili, *Intermolecular and Surface Forces*, 2nd ed. (Academic, San Diego, 1992).
- ²H. D. Ackler, R. H. French, and Y.-M. Chiang, *J. Colloid Interface Sci.* **179**, 460 (1996).
- ³D. Tabor and R. H. S. Winterton, *Proc. R. Soc. London* **312**, 435 (1969).
- ⁴H. C. Hamaker, *Physica (Amsterdam)* **4**, 1058 (1937).
- ⁵J. E. Stern, B. D. Terris, H. J. Mamin, and D. Rugar, *Appl. Phys. Lett.* **53**, 2717 (1988).
- ⁶Y. Martin and K. K. Wickramasinghe, *Appl. Phys. Lett.* **50**, 1455 (1987).
- ⁷A. L. Weisenhorn, P. K. Hansma, T. R. Albrecht, and C. F. Quate, *Appl. Phys. Lett.* **54**, 2651 (1989).
- ⁸F. London, *Trans. Faraday Soc.* **33**, 8 (1937).
- ⁹B. V. Derjaguin, *Kolloid Z.* **69**, 155 (1934).
- ¹⁰C. Argento, A. Jagota, and W. C. Carter, *J. Mech. Phys. Solids* (accepted for publication).
- ¹¹U. Hartmann, *J. Vac. Sci. Technol. B* **9**, 465 (1991).
- ¹²T. J. Senden, C. J. Drummond, and P. Kékicheff, *Langmuir* **10**, 358 (1994).
- ¹³S. Biggs and P. Mulvaney, *J. Chem. Phys.* **100**, 8501 (1994).
- ¹⁴W. A. Ducker and D. R. Clarke, *Colloids Surf. A* **94**, 275 (1994).
- ¹⁵MATHEMATICA®, Wolfram Research, Inc., telephone no. 1-800-441-6284.
- ¹⁶W. A. Ducker (personal communication).
- ¹⁷Ya. I. Rabinovich and N. V. Churaev, *Russ. J. Phys. Chem.* **52**, 256 (1990).
- ¹⁸C. J. Drummond and T. J. Senden (unpublished).
- ¹⁹R. H. French, R. M. Cannon, L. K. DeNoyer, and Y.-M. Chiang, *Solid State Ion.* **75**, 13 (1995).